SCIENTIFIC REPORTS

OPEN

SUBJECT AREAS:
CHEMISTRY
MATERIALS SCIENCE

Received
23 September 2014

Accepted
12 November 2014

Published
27 November 2014

Correspondence and requests for materials should be addressed to C.S. (csun@iphy.ac.cn)

Experimental visualization of the diffusion pathway of sodium ions in the $Na_3[Ti_2P_2O_{10}F]$ anode for sodium-ion battery

Zhaohui Ma[1], Yuesheng Wang[1], Chunwen Sun[1], J. A. Alonso[2], M. T. Fernández-Díaz[3] & Liquan Chen[1]

[1]Key Laboratory for Renewable Energy, Beijing Key Laboratory for New Energy Materials and Devices, Beijing National Laboratory for Condensed Matter Physics, Institute of Physics, Chinese Academy of Sciences, Beijing 100190, China, [2]Instituto de Ciencia de Materiales de Madrid, CSIC, Cantoblanco 28049 Madrid, Spain, [3]Institut Laue Langevin, BP 156X, Grenoble Cedex, France.

Sodium-ion batteries have attracted considerable interest as an alternative to lithium-ion batteries for electric storage applications because of the low cost and natural abundance of sodium resources. The materials with an open framework are highly desired for Na-ion insertion/extraction. Here we report on the first visualization of the sodium-ion diffusion path in $Na_3[Ti_2P_2O_{10}F]$ through high-temperature neutron powder diffraction experiments. The evolution of the Na-ion displacements of $Na_3[Ti_2P_2O_{10}F]$ was investigated with high-temperature neutron diffraction (HTND) from room temperature to 600°C; difference Fourier maps were utilized to estimate the Na nuclear-density distribution. Temperature-driven Na displacements indicates that sodium-ion diffusion paths are established within the *ab* plane. As an anode for sodium-ion batteries, $Na_3[Ti_2P_2O_{10}F]$ exhibits a reversible capacity of ~100 mAh g^{-1} with lower intercalation voltage. It also shows good cycling stability and rate capability, making it promising applications in sodium-ion batteries.

Large-scale electric energy storage (EES) requires battery systems not only to have sufficient storage capacity but also to be cost-effective and environmentally friendly[1–3]. In recent years, sodium-ion (Na^+) batteries have attracted considerable interest as an alternative to lithium-ion (Li^+) batteries for electric storage applications because of the low cost and natural abundance of sodium resources[4,5]. In this context, new advanced energy materials are required to enable the technology. Although a lot of transition metal oxides[6–11], phosphate[12–15], fluorophosphates[16,17], hexacynides[5,18,19], polymers[20], alloys[21–25], sulfid[26], red and black phosphorus[27], organic compounds[28] and carbon-based materials[29–32] have demonstrated considerable capacity and cycling ability for Na^+ insertion-extraction reaction, their energy densities and rate capabilities are far from the requirement of battery applications, because Na-ion has a much larger radius (1.02 Å) than Li-ion (0.76 Å), which leads to a sluggish kinetics of the Na-ion transport. Therefore, the materials with an open framework are highly desired for designing high-performance sodium-ion batteries. Li *et al.*[33] reported a new oxyfluorinated titanium phosphate, $Na_3[Ti_2P_2O_{10}F]$ with a higher ionic conductivity of 1.0×10^{-4} S cm^{-1} at 200°C, comparable to that of the NASICON type titanium phosphate[34]. In addition, the framework structure in $Na_3[Ti_2P_2O_{10}F]$ is quite open due to the long Ti–F–Ti distance (~4.3 Å), which may be suitable for Na^+ insertion-extraction reaction. To our knowledge, the study of the Na-ion pathways and the evolution with temperature of Na-ion motions in $Na_3[Ti_2P_2O_{10}F]$ has not yet been addressed by neutron powder diffraction (NPD). There are no reports on $Na_3[Ti_2P_2O_{10}F]$ as an electrode for Na-ion batteries.

Herein, we report on the first visualization of the sodium-ion diffusion path in $Na_3[Ti_2P_2O_{10}F]$ through high-temperature neutron powder diffraction experiments. Temperature-driven Na displacements indicate that sodium ion follow well-established diffusion paths within the *ab* plane. Furthermore, the feasibility of $Na_3[Ti_2P_2O_{10}F]$ as an anode for sodium-ion battery was examined as well. The preliminary results demonstrate $Na_3[Ti_2P_2O_{10}F]$ is a promising anode material for Na-ion batteries with a high capacity, good cycling stability and rate capability.

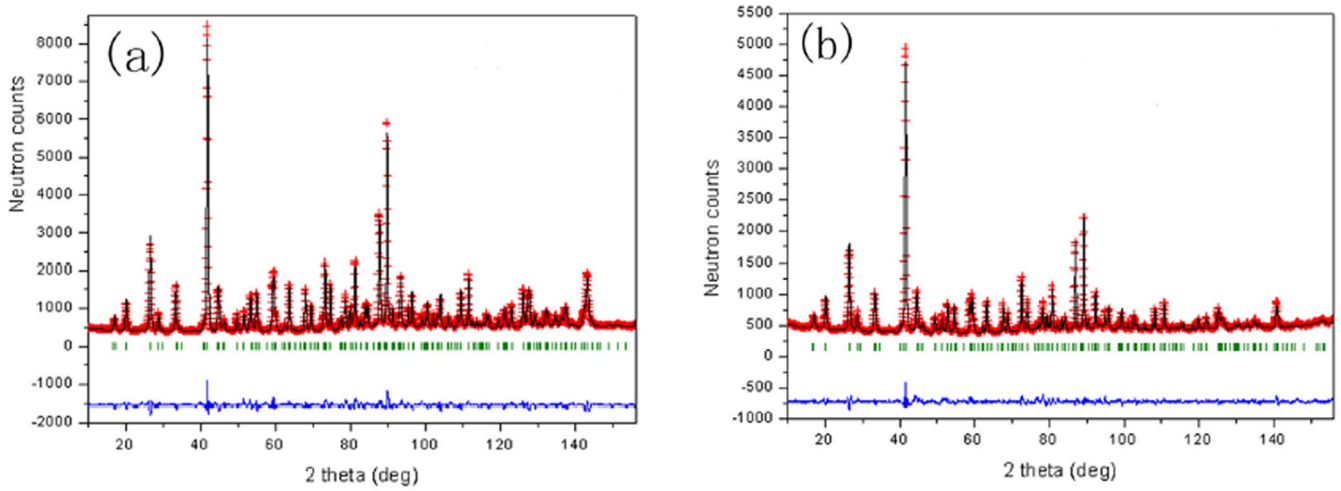

Figure 1 | Observed (crosses), calculated (line), and difference (bottom) neutron-diffraction patterns of the tetragonal $Na_3[Ti_2P_2O_{10}F]$ at room temperature (a) and 600°C (b).

Results

Structures of the as-prepared $Na_3[Ti_2P_2O_{10}F]$. The structural refinement was performed from room-temperature (RT) neutron powder diffraction (NPD) data. As reported in the Ref. 33, $Na_3[Ti_2P_2O_{10}F]$ with a tetragonal *I4/mmm* space group was considered as a starting structural model. The unit-cell parameters at RT are $a = 6.41763(8)$ Å and $c = 10.6636(2)$ Å, in good agreement with the literature[33]. In this model Ti atoms are placed at 4*e* (0, 0, z) positions, P at 4*d* (0, ½, 3/4), F at 2*a* (0, 0, 0), O1 at 4*e*, O2 at 16*n* (0, y, z) and Na at 8*h* (0, y, y) positions. Isotropic displacement factors were refined for all the atoms, excepting Na for which an anisotropic refinement was considered. Also the Na occupancy was refined; there is a slight deficiency (2.84(3) Na atoms per formula unit) with respect to the nominal value of 3. Figure 1a shows a good agreement between the observed and calculated NPD patterns. The refined structural parameters at RT are summarized in Table 1, while the main bond distances and bond valences are gathered in Table S1 in Supporting Information.

Figure 2 shows a schematic view of the crystal structure of $Na_3[Ti_2P_2O_{10}F]$. The structure consists of layers of TiO_5F octahedra and PO_4 tetrahedra sharing corners; Na atoms are interleaved between the layers. TiO_5F octahedra contain four Ti–O1 equatorial distances of 2.0108(1) Å, a very short Ti–O2 axial bond length of 1.699(4) Å which can be considered as a titanyl Ti–O terminal double bond in the framework[33] and an opposite Ti–F bond of 2.111(3) Å. Within the tetrahedron P–O1 distances take values of 1.5323(9) Å, adopting an ideal tetrahedral geometry. Na atoms present a sevenfold coordination environment with four Na–O1 bond-lengths (2.501(2) Å), two Na–O2 bonds (2.539(3) Å) and a weak bond to F (2.505(3) Å); as a reference in NaF, the Na–F distance is 2.316 Å. Figure 2b shows a projection of the structure along the c axis, which can be described as a repeat stacking of a buckled square-net sheet. As mentioned above, the Ti–O2 double bond contains a terminal oxygen that does not contribute to the connection between the sheets. The square-net sheets are interconnected thereby only through sharing F atoms on $TiFO_5$ octahedra. Because of the long Ti–F–Ti distance (~4.3 Å), the framework structure is quite open, containing two-dimensional (2D) channels where Na atoms are located.

It is interesting to evaluate the actual oxidation states of the different cations present in the solid by means of the Brown's bond valence theory[33,35], from the observed metal-oxygen or metal-fluorine distances listed in Table S1. The valence is the sum of the individual bond valences (s_i); bond valences are calculated as $s_i = \exp[(r_0 - r_i)/0.37]$. Starting from r_0 values indicated in Table S1, we obtain valences at RT of 0.986(13), 4.119(15) and 5.029(5) for Na, Ti and P, respectively, which are in excellent agreement with those expected for those cations.

In order to clarify the Na distribution and how Na ion is transported in the framework, we have undertaken a high-temperature neutron diffraction (HTND) of $Na_3[Ti_2P_2O_{10}F]$ from RT to 600°C. No structural transition was observed in the temperature range studied; the crystal structures can be refined within the same tetragonal structural model. Figure 1b illustrates the goodness of the fit at 600°C; the atomic parameters for the refinements and the Rietveld plots at 200 and 400°C are shown in Table S2 and Figure

Table 1 | Fractional atomic coordinates and isotropic or equivalent isotropic displacement parameters (Å²) for $Na_3[Ti_2P_2O_{10}F]$ from NPD data at RT. Space group *I4/mmm*, unit cell parameters $a = 6.41763$ (8) Å, $c = 10.66360$ (16) Å, $V = 439.19$ (1) Å³, $Z = 4$. Discrepancy factors: $R_p = 3.49\%$; $R_{wp} = 4.50\%$, $R_{exp} = 1.67\%$, $\chi^2 = 7.26$, $R_B = 4.34\%$

	site	*x*	*y*	*z*	U_{iso}*/U_{eq}	Occ. (<1)
Na1	8*h*	0.2760 (5)	0.2760 (5)	0.00000	0.048 (3)	0.714 (11)
Ti	4*e*	0.00000	0.00000	0.1980 (3)	0.0068 (8)*	
O1	16n	0.00000	0.30816 (14)	0.16445 (9)	0.0058 (4)*	
O2	4e	0.00000	0.00000	0.35731 (19)	0.0117 (5)*	
P	4*d*	0.00000	0.50000	0.25000	0.0004 (5)*	
F	2*a*	0.00000	0.00000	0.00000	0.0079 (7)*	

Atomic displacement parameters (Å²)

	U^{11}	U^{22}	U^{33}	U^{12}	U^{13}	U^{23}
Na1	0.067 (3)	0.067 (3)	0.010 (2)	−0.045 (3)	0.00000	0.00000

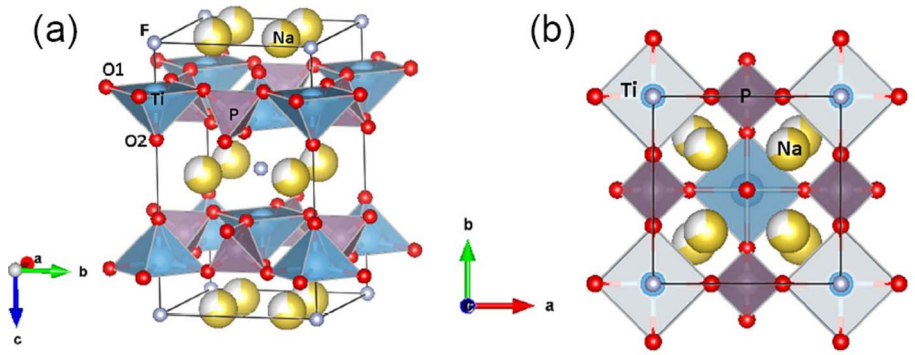

Figure 2 | **Crystal structure of tetragonal $Na_3[Ti_2P_2O_{10}F]$ observed (a) approximately along the a axis and (b) along the c axis.**

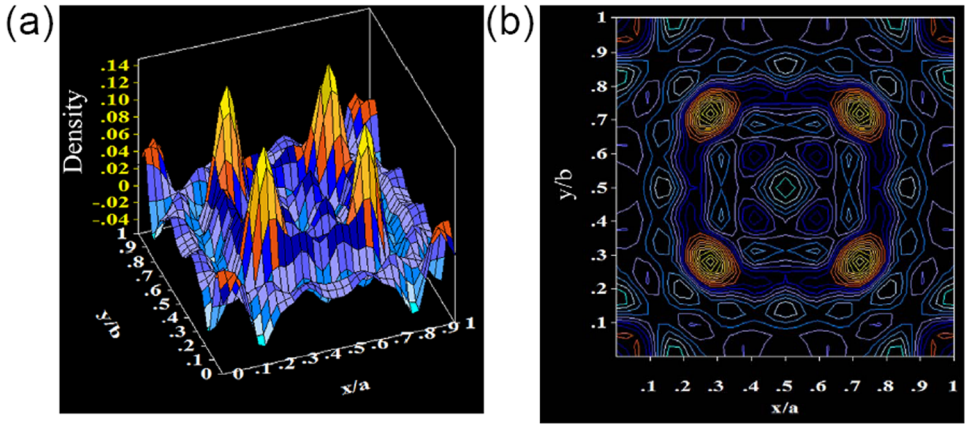

Figure 3 | (a) Difference Fourier maps in a model where Na has been removed. Na1 peaks are clearly located at 8 h sites, but there is intermediate nuclear density between the peaks, indicating Na is delocalized on the *ac* plane.

S1 in the Supporting Information. An interesting insight into the Na ion motion was achieved by removing Na atoms from the structural model at 600°C and performing a difference Fourier synthesis from the observed and calculated NPD data. The difference contains information of the missing scattering density (in this case nuclear density). Figure 3 shows a difference Fourier map corresponding to the $z = 0$ section where strong positive peaks corresponding to the 8*h* sites for Na1 are observed, and some intermediate nuclear density is observed between both peaks, indicating that Na is partially delocalized at intermediate positions. It can be visualized clearly in Figure 4, where Na atoms are delocalized in octagonal rings within the interlayer space, suggesting that the diffusion is two dimensional (2D), since there is no residual Na scattering through the layers even at an elevated temperature of 600°C.

Furthermore, at higher temperatures the Na displacement factors become very anisotropic, as shown in Figure 5. Looking at one *ab* layer, we see that the Na ellipsoids are elongated along the unit-cell diagonals, suggesting that a jump from Na sites at adjacent unit cells is possible, thus allowing the 2D motion. They jump though a wide window formed by two F^- ions very far apart (≈6.4 Å), so the potential barrier to prevent this jump is very low. Based on the NPD results, we propose that the sodium ion diffusion paths may follow a trajectory through the *ab* plane, as shown in Figure 5b.

Electrochemical properties of $Na_3[Ti_2P_2O_{10}F]$. The sodium-ion insertion/extraction properties of the $Na_3[Ti_2P_2O_{10}F]$ as an anode material were investigated by galvanostatic charge-discharge measurements over a voltage range of 0 to 2.5 V versus Na^+/Na. Figure 6a shows the charge (Na^+ extraction)/discharge (Na^+ insertion) profiles at various current rates. It shows a discharge capacity of about 100 mAh g^{-1} at 10 mA g^{-1} charge/discharge rate, which is acceptable for Na-ion batteries.

The rate capability of the $Na_3[Ti_2P_2O_{10}F]$ electrode is evaluated by charging/discharging at various current densities from 10 mA g^{-1} to 200 mA g^{-1} (Figure 6b). The reversible specific capacity remains

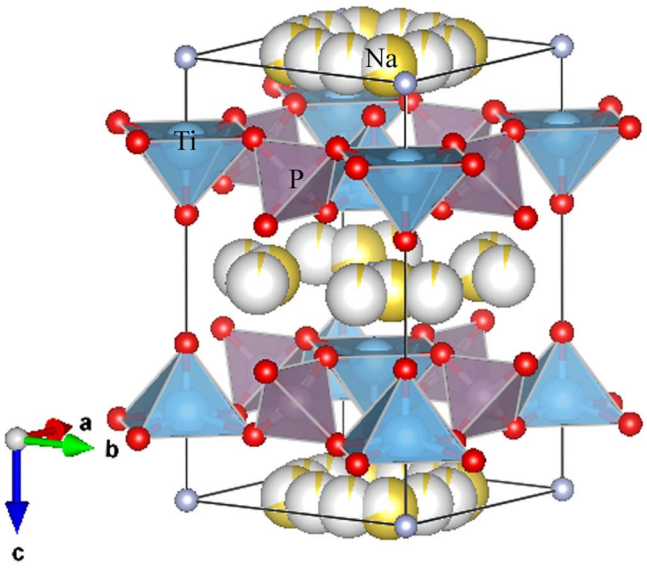

Figure 4 | **Unit cell of $Na_3[Ti_2P_2O_{10}F]$ including the Na delocalization observed by Fourier Synthesis; Na are delocalized in octagonal rings places in the interlayer space between PO_4-TiO_5F sheets.**

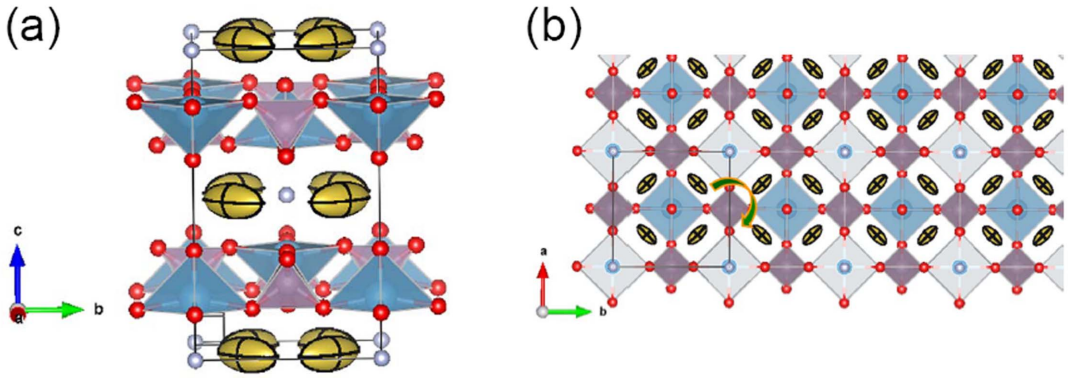

Figure 5 | (a) Enhanced anisotropic motion of Na atoms at 600°C, with the major axis of the ellipsoids (90% probability) along the diagonals of the unit cell. (b) *ab* projection suggesting the jumping path of Na^+ ions to neighboring unit cells from partially occupied 8*h* sites.

approximately 41 mAh g^{-1} at a charge/discharge rate of 100 mA g^{-1} and 26 mAh g^{-1} at a charge/discharge rate of 200 mA g^{-1}. Importantly, after the high current density testing, the capacity of the $Na_3[Ti_2P_2O_{10}F]$ electrode can recover to the initial value, indicating its high reversibility. Figure 6c shows the cycling performance of the $Na_3[Ti_2P_2O_{10}F]$ electrode at a current density of 100 mA g^{-1}. The reversible specific capacity of the $Na_3[Ti_2P_2O_{10}F]$ electrode keeps almost stable. Simultaneously, the Coulombic efficiency keeps above 98% after 20 cycles. These results clearly demonstrate that the $Na_3[Ti_2P_2O_{10}F]$ is a promising candidate for practical applications in sodium ion batteries.

Discussion

$Na_3[Ti_2P_2O_{10}F]$ has an interesting framework structure consisting of $TiFO_5$ octahedra and PO_4 tetrahedra. The $TiFO_5$ octahedra and PO_4 tetrahedra are alternatively linked via sharing four oxygen atoms (in the *ac* plane)[33]. The square-net sheets are interconnected thereby only through sharing F atoms on $TiFO_5$ octahedra. The framework structure in $Na_3[Ti_2P_2O_{10}F]$ is quite open due to the long Ti–F–Ti distance (~4.3 Å). The temperature-driven Na displacements indicate that sodium ion diffusion paths follow a trajectory through the *ab* plane. Moreover, as an anode for sodium-ion batteries, $Na_3[Ti_2P_2O_{10}F]$ exhibits a reversible capacity of ~100 mAh g^{-1} with lower intercalation voltage. It also shows good cycling stability and rate capability, making it a promising anode for sodium-ion batteries.

Methods

Materials synthesis. Pure phase $Na_3[Ti_2P_2O_{10}F]\cdot xH_2O$ were obtained by a modified hydrothermal method as reported by Li *et al.*[33]. In a typical synthesis, a mixture of 6.00 g of $Ti(SO_4)_2$, 36.0 g of $NaBO_3\cdot 4H_2O$, and 19.0 g of $NH_4H_2PO_4$, together with 3.0 g of $NaBF_4$ and 20.0 mL distilled water, was put into a 100 mL Teflon-lined stainless steel autoclave. The autoclave was sealed, heated to 200°C under autogenous pressure for 2 days, and then cooled to room temperature naturally. The white precipitate was isolated by washing with hot distilled water and drying it at ambient temperature. The obtained product was calcined at 650°C in Ar atmosphere for 2 hours to get the final product $Na_3[Ti_2P_2O_{10}F]$. For improving the low electronic conductivity of $Na_3[Ti_2P_2O_{10}F]$, the product obtained by hydrothermal synthesis was mixed with Ketjen black (KB) using ball-milling. After calcination at 500°C for 2 h in

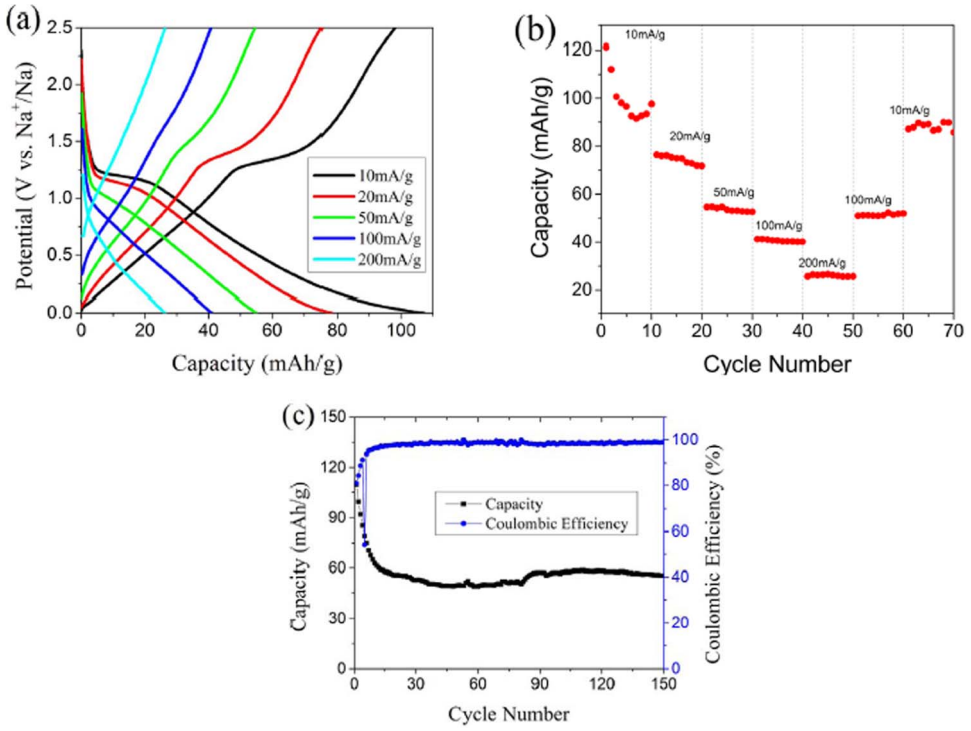

Figure 6 | **Sodium storage performance of $Na_3[Ti_2P_2O_{10}F]$ electrodes.** (a) The charge/discharge profiles at various current rates in the voltage range of 0 to 2.5 V versus Na^+/Na; (b) Rate capability: the capacity versus cycle number at various current rates; (c) Long-term cycling performance: the capacity and Coulombic efficiency versus cycle number at a current rate of 100 mA g^{-1}.

Ar, the $Na_3[Ti_2P_2O_{10}F]$ coated with carbon was obtained. The amount of carbon was about 7wt% after ball-milling.

Characterizations. XRD analyses were performed on a D8-Advance diffractometer with Cu Kα radiation (λ = 1.54 Å). The amount of carbon was analyzed by induced coupled plasma- atomic emission spectrometer (ICP-AES, Thermo Electron Corporation). NPD patterns were collected at the D2B diffractometer of the Institut Laue-Langevin, Grenoble, with a wavelength λ = 1.594 Å within the 2θ range from 10 to 153° at 25, 200, 400, and 600°C. About 2 g of the sample were contained in a vanadium cylinder. For the T ≥ 200°C collection, the sample was placed in the isothermal zone of a furnace with a vanadium resistor operating under vacuum ($P_{O2} \approx 1 \times 10^{-6}$ Torr). In all cases a time of 3 h was required to collect a full diffraction pattern. The NPD data were analyzed by the Rietveld method with the FULLPROF program[36]. A pseudo-Voigt function was chosen to generate the line shape of the diffraction peaks. The irregular background coming from the quartz container was extrapolated from points devoid of reflections.

Electrochemical measurements. The working electrode was prepared by spreading the slurry of the active materials (75wt%), acetylene black (15wt%) and the polyvinylidene fluoride (10wt%) binder on a Cu foil. Considering the carbon coating in the active material, the actual mass ratio of the $Na_3[Ti_2P_2O_{10}F]$: carbon: binder is about 7 : 2 : 1. The working electrodes were dried at 100°C under vacuum for 10 h. The electrolyte for Na-ion batteries is 1M $NaClO_4$ in EC : DEC (4 : 6 in volume). The coin-type (CR2032) cells were assembled with pure sodium foil as a counter electrode, and a glass fiber as the separator in an argon-filled glove box. The charge and discharge measurements were carried out on a Land BT2000 battery test system (Wuhan, China) in a voltage range of 0–2.5 V under room temperature. Cyclic voltammetry (CV) was measured using Autolab PGSTA128N at a scan rate of 0.04 mV/s in a voltage range of 0–2.5 V versus Na^+/Na.

1. Armand, M. & Tarascon, J. M. Building better batteries. *Nature* **451**, 652–657 (2008).
2. Goodenough, J. B. & Kim, Y. Challenges for rechargeable Li batteries. *Chem. Mater.* **22**, 587–603 (2010).
3. Sun, C., Rajasekhara, S., Goodenough, J. B. & Zhou F. Monodisperse porous $LiFePO_4$ microspheres for a high power Li-ion battery cathode. *J. Am. Chem. Soc.* **133**, 2132–2135 (2011).
4. Palomares, V. *et al.* Na-ion batteries, recent advances and present challenges to become low cost energy storage systems. *Energy & Environ. Sci.* **5**, 5884–5901 (2012).
5. Qian, J. F., Zhou, M., Cao, Y. L., Ai, X. P. & Yang, H. X. Nanosized $Na_4Fe(CN)_6$/C composite as a low-cost and high-rate cathode material for sodium-ion batteries. *Adv. Energy Mater.* **2**, 410–414 (2012).
6. Cao, Y. *et al.* Reversible sodium ion insertion in single crystalline manganese oxide nanowires with long cycle life. *Adv. Mater.* **23**, 3155–3160 (2011).
7. Kim, D. *et al.* Enabling sodium batteries using lithium-substituted sodium layered transition metal oxide cathodes. *Adv. Energy Mater.* **1**, 333–336 (2011).
8. Wang, Y. *et al.* A zero-strain layered metal oxide as the negative electrode for long-life sodium-ion batteries. *Nature Commun.* **4**, 2365 (2013).
9. Yuan, D. *et al.* A honeycomb-layered $Na_3Ni_2SbO_6$: a high-rate and cycle-stable cathode for sodium-ion batteries. *Adv. Mater.* **26**, 6301–6306 (2014).
10. Zhao, L., Pan, H., Hu, Y., Li, H. & Chen, L. Spinel lithium titanate ($Li_4Ti_5O_{12}$) as novel anode material for room-temperature sodium-ion battery. *Chin. Phys. B.* **21**, 028201 (2012).
11. Pan, H. *et al.* Sodium storage and transport properties in layered $Na_2Ti_3O_7$ for room-temperature sodium-ion battery. *Adv. Energy Mater.* **3**, 1186–1194 (2013).
12. Jian, Z. *et al.* Carbon coated $Na_3V_2(PO_4)_3$ as novel electrode material for sodium ion batteries. *Electrochem. Commun.* **14**, 86–89 (2012).
13. Saravanan, K., Mason, C. W., Rudola, A., Wong, K. H. & Balaya, P. The first report on excellent cycling stability and superior rate capability of $Na_3V_2(PO_4)_3$ for sodium ion batteries. *Adv. Energy Mater.* **3**, 444–450 (2012).
14. Fang, Y. *et al.* Mesoporous amorphous $FePO_4$ nanospheres as high-performance cathode material for sodium-ion batteries. *Nano Lett.* **14**, 3539–3543 (2014).
15. Song, J., Xu, M., Wang, L. & Goodenough, J. B. Exploration of $NaVOPO_4$ as a cathode for a Na-ion battery. *Chem. Commun.* **49**, 5280–5285 (2013).
16. Ellis, B. L., Makahnouk, W. R. M., Makimura, Y., Toghill, K. & Nazar, L. F. A multifunctional 3.5 V iron-based phosphate cathodes for rechargeable batteries. *Nature Mater.* **6**, 749–753 (2007).
17. Xu, M. *et al.* $Na_3V_2O_2(PO_4)_2F$/graphene sandwich structure for high-performance cathode of a sodium-ion battery, *Phys.Chem. Chem. Phys.* **15**, 13032–13037 (2013).
18. Lu, Y., Wang, L., Cheng, J. & Goodenough, J. B. Prussian blue: a new framework of electrode materials for sodium batteries. *Chem. Commun.* **48**, 6544–6546 (2012).
19. Wang, L. *et al.* A superior low-cost cathode for a Na-ion battery. *Angew. Chem. Int. Ed.* **52**, 1964–1967 (2013).
20. Zhao, R., Zhu, L., Cao, Y., Ai, X. & Yang, H. An aniline-nitroaniline copolymer as a high capacity cathode for Na-ion batteries. *Electrochem. Commun.* **21**, 36–38 (2012).
21. Abel, P. R., Fields, M. G., Heller, A. & Mullins, C. B. Tin-germanium alloys as anode materials for sodium-ion batteries. *ACS Appl. Mater. Interfaces* **6**, 15860–15867 (2014).
22. Mortazavi, M., Deng, J. K., Shenoy, V. B. & Medhekar, N. V. Elastic softening of alloy negative electrodes for Na-ion batteries. *J. Power Sources* **225**, 207–214 (2013).
23. Ji, L. W. *et al.* Controlling SEI formation on SnSb-porous carbon nanofibers for improved Na ion storage. *Adv. Mater.* **26**, 2901–2908 (2014).
24. Darwiche, A., Sougrati, M. T., Fraisse, B., Stievano, L. & Monconduit, L. Facile synthesis and long cycle life of SnSb as negative electrode material for Na-ion batteries. *Electrochem. Commun.* **32**, 18–21 (2013).
25. Xiao, L. *et al.* High capacity, reversible alloying reactions in SnSb/C nanocomposites for Na-ion battery applications. *Chem. Commun.* **48**, 3321–3323 (2012).
26. Liao, Y. H. *et al.* Sodium intercalation behavior of layered Na_xNbS_2 ($0 \le x \le 1$). *Chem. Mater.* **9**, 1699–1705 (2013).
27. Qian, J., Wu, X., Cao, Y., Ai, X. & Yang, H. High capacity and rate capability of amorphous phosphorus for sodium ion batteries. *Angew. Chem. Int. Ed.* **52**, 4633–4636 (2013).
28. Park, Y. *et al.* Sodium terephthalate as an organic anode material for sodium ion batteries. *Adv. Mater.* **24**, 3562–3567 (2012).
29. Matsuo, Y. & Ueda, K. Pyrolytic carbon from graphite oxide as a negative electrode of sodium-ion battery. *J. Power Sources.* **263**, 158–162 (2014).
30. Zhou, X. *et al.* Sb nanoparticles decorated N-rich carbon nanosheets as anode materials for sodium ion batteries with superior rate capability and long cycling stability. *Chem. Commun.* **50**, 12888–12891 (2014).
31. Wang, Y. *et al.* Reversible sodium storage via conversion reaction of a MoS_2-C composite. *Chem. Commun.* **50**, 10730–10733 (2014).
32. Hong, K. *et al.* Biomass derived hard carbon used as a high performance anode material for sodium ion batteries. *J. Mater. Chem. A* **2**, 12733–12738 (2014).
33. Yang, S. *et al.* $Na_3[Ti_2P_2O_{12}F]$: a new oxyfluorinated titanium phosphate with an ionic conductive property. *Chem. Mater.* **19**, 942–947 (2007).
34. Mouahid, F. E. *et al.* Crystal chemistry and ion conductivity of the $Na_{1+x}Ti_{2-x}Al_x(PO_4)_3$ ($0 \le x \le 0.9$) NASICON series. *J. Mater. Chem.* **10**, 2748–2753 (2000).
35. Brown, I. D. & Altermatt, D. Bond-valence parameters obtained from a systematic analysis of the inorganic crystal structure database. *Acta Cryst. B* **41**, 244–247 (1985).
36. Rodríguez-Carvajal, J. Recent advances in magnetic structure determination by neutron powder diffraction. *Phys. B* **192**, 55–69 (1993).

Acknowledgments

This work is financially supported by the National Science Foundation of China (NSFC) (Grant Nos. 51372271, 51172275) and the start up grant from Institute of Physics (IOP). J. Alonso is grateful to the Spanish Ministry of Economy and Competitiveness for granting the project MAT2013-41099-R, and ILL for making all facilities available for the neutron diffraction experiments.

Author contributions

C.W.S. conceived and designed the experiments; Z.H.M prepared the materials; Z.H.M and Y.S.W. carried out the electrochemical experiments; J.A.A. and M.T.F. did the NPD collection and analyzed the NPD data; C.W.S., L.Q.C. and J.A.A. wrote the paper; all the authors participated in analysis of the experimental data and discussion of the results and the paper.

Additional information

Supplementary information accompanies this paper at http://www.nature.com/scientificreports

Competing financial interests: The authors declare no competing financial interests.

How to cite this article: Ma, Z. *et al.* Experimental visualization of the diffusion pathway of sodium ions in the $Na_3[Ti_2P_2O_{10}F]$ anode for sodium-ion battery. *Sci. Rep.* **4**, 7231; DOI:10.1038/srep07231 (2014).